

# Limits on spin-independent couplings of WIMP dark matter with a p-type point-contact germanium detector

H.B. Li,<sup>1</sup> H.Y. Liao,<sup>1</sup> S.T. Lin,<sup>1,2</sup> S.K. Liu,<sup>3</sup> L. Singh,<sup>1,4</sup> M.K. Singh,<sup>1,4</sup> A.K. Soma,<sup>1,4</sup> H.T. Wong,<sup>1,\*</sup> Y.C. Wu,<sup>5</sup> W. Zhao,<sup>5</sup> G. Asryan,<sup>1</sup> Y.C. Chuang,<sup>1</sup> M. Deniz,<sup>2</sup> J.M. Fang,<sup>6</sup> C.L. Hsu,<sup>1</sup> T.R. Huang,<sup>1</sup> G. Kiran Kumar,<sup>1</sup> S.C. Lee,<sup>1</sup> J. Li,<sup>5</sup> J.M. Li,<sup>5</sup> Y.J. Li,<sup>5</sup> Y.L. Li,<sup>5</sup> C.W. Lin,<sup>1</sup> F.K. Lin,<sup>1</sup> Y.F. Liu,<sup>1,7</sup> H. Ma,<sup>5</sup> X.C. Ruan,<sup>8</sup> Y.T. Shen,<sup>1</sup> V. Singh,<sup>4</sup> C.J. Tang,<sup>3</sup> C.H. Tseng,<sup>1</sup> Y. Xu,<sup>1,7</sup> S.W. Yang,<sup>1</sup> C.X. Yu,<sup>1,7</sup> Q. Yue,<sup>5</sup> Z. Zeng,<sup>5</sup> M. Zeyrek,<sup>9</sup> and Z.Y. Zhou<sup>8</sup>

(TEXONO Collaboration)

<sup>1</sup> *Institute of Physics, Academia Sinica, Taipei 11529, Taiwan.*

<sup>2</sup> *Department of Physics, Dokuz Eylül University, Buca, İzmir 35160, Turkey.*

<sup>3</sup> *Department of Physics, Sichuan University, Chengdu 610065, China.*

<sup>4</sup> *Department of Physics, Banaras Hindu University, Varanasi 221005, India.*

<sup>5</sup> *Department of Engineering Physics, Tsinghua University, Beijing 100084, China.*

<sup>6</sup> *Kuo-Sheng Nuclear Power Station, Taiwan Power Company, Kuo-Sheng 207, Taiwan.*

<sup>7</sup> *Department of Physics, Nankai University, Tianjin 300071, China.*

<sup>8</sup> *Department of Nuclear Physics, Institute of Atomic Energy, Beijing 102413, China.*

<sup>9</sup> *Department of Physics, Middle East Technical University, Ankara 06531, Turkey.*

(Dated: March 6, 2013)

We report new limits on spin-independent WIMP-nucleon interaction cross-section using 39.5 kg-days of data taken with a p-type point-contact germanium detector of 840 g fiducial mass at the Kuo-Sheng Reactor Neutrino Laboratory. Crucial to this study is the understanding of the selection procedures and, in particular, the bulk-surface events differentiation at the sub-keV range. The signal-retaining and background-rejecting efficiencies were measured with calibration gamma sources and a novel n-type point-contact germanium detector. Part of the parameter space in cross-section versus WIMP-mass implied by various experiments is probed and excluded.

PACS numbers: 95.35.+d, 29.40.-n, 98.70.Vc

About one quarter of the energy density of the universe can be attributed to Cold Dark Matter(CDM)[1], whose nature and properties are unknown. Weakly Interacting Massive Particles (WIMP, denoted by  $\chi$ ) are the leading candidates for CDM. There are intense efforts to look for WIMPs through direct detection of nuclear recoils in terrestrial experiments via  $\chi N \rightarrow \chi N$  elastic scattering.

Most experimental programs are optimized to study WIMPs with mass  $m_\chi \sim 10-100$  GeV, motivated by popular supersymmetric models. Germanium detectors with sub-keV sensitivities were identified and demonstrated as possible means to probe the “low-mass” WIMPs with  $m_\chi < 10$  GeV[2]. This inspired development of p-type point-contact germanium detectors (PPCGe) which provide such sensitivities with modular mass of kg-scale[3].

Our earlier measurements at the Kuo-Sheng Reactor Neutrino Laboratory (KSNL, with a shallow depth of about 30 meter-water-equivalence) using a 4-element array with a total mass of 20 g and analysis threshold of 220 eVee (“ee” denoting electron-equivalence energy throughout) have placed constraints on  $m_\chi > 3$  GeV[4]. The CoGeNT experiment reported data with a 440 g PPCGe[5], showing an excess of events at the sub-keV range over the background models. A consistent annual modulation signature was observed. Allowed region in the spin-independent  $\chi N$  couplings ( $\sigma_{\chi N}^{\text{SI}}$ ) was derived. Intense interest and theoretical speculations in the low-mass WIMP region were generated, some of

which explored the consequences of additional corrections on residual sub-keV surface background[6]. The low energy data of the CDMS and XENON experiments[7] have subsequently excluded the allowed region with different detector techniques, though these interpretations were challenged[8], and the issue remains controversial. It is crucial to have independent experiments which can probe the CoGeNT allowed region and provide further understanding on the detector response and the nature of the sub-keV events in PPCGe.

We report new results at the sub-keV region with a PPCGe having a fiducial mass of 840 g (actual crystal mass 926 g) at KSNL. The low-background facilities as well as the hardware, trigger and data acquisition (DAQ) configurations were described in our previous work[4, 9]. The PPCGe detector was enclosed by an NaI(Tl) anti-Compton (AC) detector and passive shieldings of OFHC (oxygen free high conductivity) copper inside a plastic bag purged by nitrogen gas evaporated from the liquid nitrogen dewar. This set-up was further shielded by, from inside out, 5 cm of OFHC copper, 25 cm of boron-loaded polyethylene, 5 cm of steel and 15 cm of lead. This structure was surrounded by cosmic-ray (CR) veto panels made of plastic scintillators read out by photomultipliers. Both AC and CR signals are crucial, serving both as vetos to reject background and as tags to identify samples for efficiency measurements.

Signals from the PPCGe point-contact are supplied

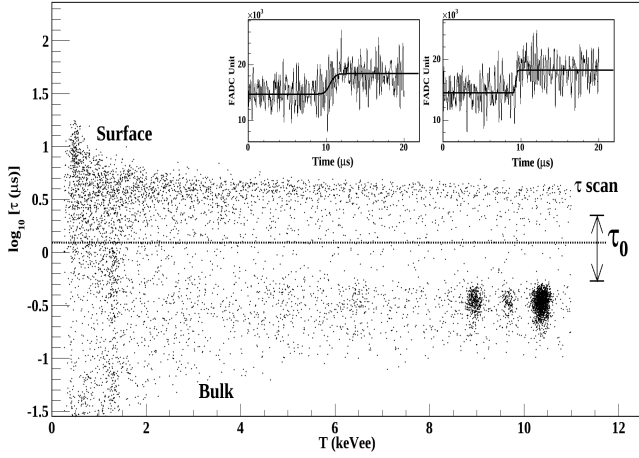


FIG. 1: Scatter plot of the PPCGe rise time ( $\log_{10}[\tau]$ ) versus energy. The  $\tau_0$ -line corresponds to the BS cut in this analysis, with the range for cut-stability test ( $\tau$ -scan) indicated. Typical B and S pulses at  $\sim 700$  eVee are depicted in the insets.

through a reset preamplifier. The output is distributed to a timing amplifier (TA) which keeps the fast rise-time information, and to shaping amplifiers at both  $6 \mu\text{s}$  ( $\text{SA}_6$ ) and  $12 \mu\text{s}$  ( $\text{SA}_{12}$ ) shaping time which provide energy information and the triggers. Signals from the PPCGe outer surface-electrode are processed with a resistive feedback preamplifier and followed by a shaping amplifier at  $4 \mu\text{s}$  shaping time ( $\text{SA}_{\text{out}}$ ). The TA,  $\text{SA}_{6,12,\text{out}}$ , and AC-NaI(Tl) output were digitized by flash analog-to-digital converters at 200 MHz, 60 MHz and 20 MHz, respectively. The discriminator and timing outputs of the CR panels were also recorded. The trigger threshold was adjusted such that the trigger efficiency is 100% above 300 eVee, verified by test pulser (TST) events. A total of 53.8 days of data were taken, where the DAQ dead time was 12.6%, measured by random trigger (RT) events. Energy calibration was achieved by the internal X-ray peaks with the zero-energy defined by the pedestals provided by the RT events, while the range in between was cross-checked with TST events.

A cut-based analysis was adopted. There are three categories of selection criteria: (i) the “physics versus noise events” (PN) cuts differentiate physics signals from spurious electronic noise; (ii) the CR and AC cuts identify events with activities only at the PPCGe; and (iii) the “bulk versus surface events” (BS) cut selects events at the interior of PPCGe. In addition, the efficiencies and suppression factors ( $\epsilon_X, \lambda_X$ ) for every selection ( $X=\text{PN}, \text{AC}, \text{CV}, \text{BS}$ ) are measured. They correspond to the probabilities of (signal, background) events being correctly identified. Only events above the electronics noise-edge of 500 eVee were adopted in this analysis. The physics samples selected by the PN cuts are categorized by “ACV(T)+CRV(T)+B(S)”, where ACV(T) and CRV(T) are, respectively, the

AC- and CR-vetoed(tagged) events which are in anti-coincidence(coincidence) with the PPCGe signals, while B(S) denote the bulk(surface) samples. The  $\chi\text{N}$  candidates would therefore manifest as ACV+CRV+B events.

Background suppression with the PN, AC and CR cuts and the evaluations of their respective ( $\epsilon_X, \lambda_X$ ) follow the well-studied procedures as in earlier experiments[4, 9, 10]. The PN cuts are based on pulse shape characteristics and correlations in ( $\text{TA}, \text{SA}_6, \text{SA}_{12}, \text{SA}_{\text{out}}$ ). They suppress spurious triggers induced by microphonics effects or the tails of pedestal fluctuations. Background induced by the preamplifier reset are identified by the timing correlations with the reset instant. The *in situ* doubly-tagged ACT+CRT events serve as the physics reference samples, with which the signal efficiencies  $\epsilon_{PN}$  shown in Figure 2c are accurately measured. The majority of the electronics-induced events above noise-edge are identified ( $\lambda_{PN} \sim 1$ ). The efficiencies for AC and CR selections are measured by RT events to be, respectively,  $\epsilon_{AC} > 0.99$  and  $\epsilon_{CR} = 0.93$ . The suppressions are  $\lambda_{AC} = 1.0$  above the NaI(Tl) threshold of 20 keVee, while  $\lambda_{CR} = 0.92$ , measured by reference cosmic samples in which the energy depositions at NaI(Tl) are above 20 MeVee.

The BS selection, on the other hand, is a unique feature to PPCGe. The surface-electrode of PPCGe is a lithium-diffused  $n^+$  layer of mm-scale thickness. Partial charge collection in the surface layer (S) gives rise to reduced measureable energy and slower rise-time, as compared to those in the bulk region (B)[5, 11, 12]. The thickness of the S layer was derived to be  $l_S = 1.16$  mm, via the comparison of simulated and observed intensity ratios of  $\gamma$ -peaks from a  $^{133}\text{Ba}$  source[13]. This gives rise to a fiducial mass of 840 g, or a data size of 39.5 kg-days.

The data are differentiated in B/S event-by-event through the rise-time ( $\tau$ ) of their TA output. The  $\log_{10}[\tau]$  versus measured energy( $T$ ) scatter plot and examples of typical B/S events are depicted in Figure 1. The observed and actual rates are denoted by ( $B', S'$ ) and ( $B, S$ ), respectively. The B&S bands are well separated at  $T > 2$  keVee, such that ( $\epsilon_{BS}, \lambda_{BS}$ )  $\sim$  (100%, 100%), or equivalently,  $B=B'$  and  $S=S'$ . At lower energy, ( $B', S'$ ) and ( $B, S$ ) are related by the coupled equations:

$$\begin{aligned} B' &= \epsilon_{BS} \cdot B + (1 - \lambda_{BS}) \cdot S \\ S' &= (1 - \epsilon_{BS}) \cdot B + \lambda_{BS} \cdot S, \end{aligned} \quad (1)$$

with an additional unitarity constrain:  $B+S=B'+S'$ .

To evaluate ( $\epsilon_{BS}, \lambda_{BS}$ ) at sub-keV energy, it is necessary to devise calibration schemes which provide at least two measurements of ( $B', S'$ ) where ( $B, S$ ) are independently known. The TST events are inappropriate since their TA-output exhibit different pulse shapes from those of physics events. Instead three complementary data samples, as displayed in Figure 2a, were adopted:

(I) Surface-rich events with  $\gamma$ -ray sources – Calibrations with both high and low energy  $\gamma$ -sources ( $^{241}\text{Am}$

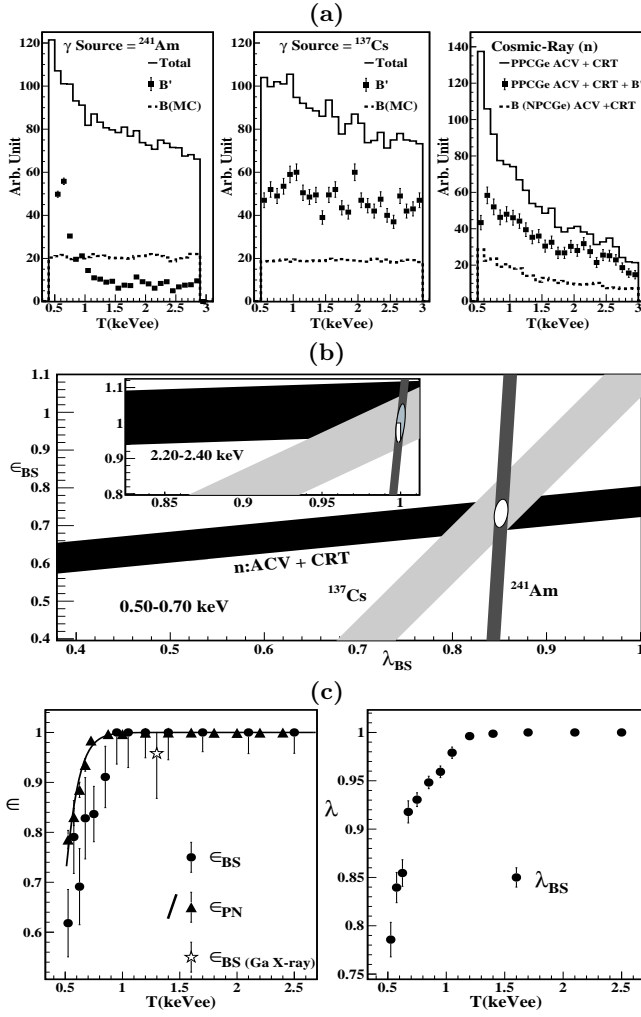


FIG. 2: The derivation of  $(\epsilon_{BS}, \lambda_{BS})$ — (a) Total, B' and B spectra from the surface-rich  $\gamma$ -ray ( $^{241}\text{Am}$ ,  $^{137}\text{Cs}$ ) and bulk-rich cosmic-ray induced neutron calibration data. The relative normalizations between (B,B') are fixed by  $\epsilon_{BS}=100\%$  at  $T>2.5$  keVee. (b) Allowed bands of  $(\epsilon_{BS}, \lambda_{BS})$  at threshold and at a high energy band. (c) The measured  $(\epsilon_{BS}, \lambda_{BS})$  and  $\epsilon_{PN}$  as a function of energy.

at 60 keVee and  $^{137}\text{Cs}$  at 662 keVee, respectively) were performed to characterize the PPCGe response. As displayed in Figure 2a, the measured B'-spectra are compared to the reference B derived from full simulation with  $l_S=1.16$  mm as input. The simulated B-spectra due to external  $\gamma$ -sources over a large range of energy are flat for  $T<5$  keVee.

(II) Bulk-rich events with cosmic-ray induced fast neutrons — A 523 g first-of-its-kind n-type point-contact germanium (NPCGe) detector was constructed. The components and dimensions are identical to those of PPCGe. The surface of NPCGe is a  $p^+$  boron implanted electrode of sub-micron thickness. There are no anomalous surface effects in NPCGe. Data were taken under identical shielding configurations as the PPCGe at

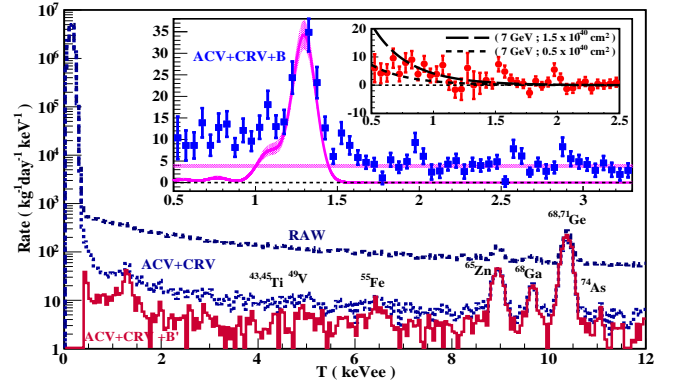


FIG. 3: Measured energy spectra of PPCGe, showing the raw spectra and those after ACV+CRV cut, as well as +B'. The large inset shows the  $(\epsilon_{BS}, \lambda_{BS})$ -corrected ACV+CRV+B spectrum, with a flat background and L-shell X-ray peaks overlaid. The small inset depicts the residual spectrum superimposed with that of an allowed (excluded) cross-section at  $m_\chi=7$  GeV.

KSNL. The ACV+CRT condition selects cosmic-ray induced fast neutron events without associated  $\gamma$ -activities, which manifest mostly ( $\sim 85\%$ ) as bulk events in PPCGe. Accordingly, as depicted in Figure 2a, the measured ACV+CRT data with NPCGe is taken as the B-reference and compared with those of ACV+CRT+B' in PPCGe.

Using calibration data (I) and (II),  $(\epsilon_{BS}, \lambda_{BS})$  are evaluated by solving the coupled equations in Eq. 2. As examples, the three allowed bands on  $(\epsilon_{BS}, \lambda_{BS})$  at threshold and at a high energy band are illustrated in Figure 2b. The different orientations of the bands are consequences of the different depth distributions of the samples, which give rise to different B:S ratios. The bands have common overlap regions, indicating the results are insensitive to the event locations. The surface-rich  $\gamma$ -events and the bulk-rich cosmic-ray induced neutron-events play complementary roles in constraining  $\lambda_{BS}$  and  $\epsilon_{BS}$ , respectively. The results are depicted in Figure 2c, with  $\epsilon_{PN}$  overlaid. Consistency is checked by comparing the measured strength of the *in situ* Ga-L X-ray peak at 1.3 keVee after BS-selection to that predicted by the corresponding K-peak at 10.37 keVee.

The raw spectra as well as those of ACV+CRV and ACV+CRV+B' are depicted in Figure 3. The peaks correspond to known K-shell X-rays emissions from the cosmogenically-activated isotopes. The  $(\epsilon_{BS}, \lambda_{BS})$ -corrected spectrum of ACV+CRV+B is shown in the large inset. Errors above  $\sim 800$  eV are dominated by statistical uncertainties, while those below are defined by the systematics from the calibration procedures. When the expected L-peaks and a flat  $\gamma$ -ray background are subtracted, the residual spectrum corresponds to  $\chi N$  candidate events and is shown in the small inset. In addition, the stability of the results is studied over the variations of  $\tau_0$  within the  $\tau$ -scan range of Figure 1. The corre-

TABLE I: The  $p$ -values for the stability hypothesis on the key parameters following a  $\tau$ -scan of Figure 1. The ACV+CRV+B rates are insensitive of the choice of  $\tau_0$ .

Energy Range (keVee)	0.5-0.7	1.5-1.9
$\epsilon_{BS}$	$< 10^{-5}$	$< 10^{-5}$
$\lambda_{BS}$	$< 10^{-5}$	$< 10^{-5}$
ACV+CRV+B'	0.24	0.16
ACV+CRV+S'	0.17	0.21
ACV+CRV+B	0.57	0.65

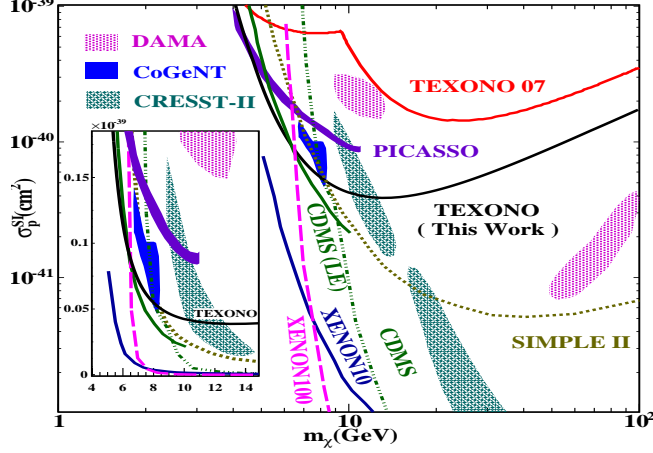


FIG. 4: Exclusion plot of spin-independent  $\chi$ -N coupling, superimposed with the results from other benchmark experiments.

sponding changes in  $(\epsilon_{BS}, \lambda_{BS}, B', S', B)$  are derived. The  $p$ -values for the stability hypothesis are listed in Table I. The ACV+CRV+B rates are stable and insensitive to the choice of  $\tau_0$ , even with  $(\epsilon_{BS}, \lambda_{BS})$  exhibiting significant variations in the expected directions. This demonstrates that the calibration procedures are valid and robust.

Constraints on  $\sigma_{\chi N}^{SI}$  are derived via standard approach with conventional astrophysical models[1] (local density of 0.3 GeV/cc and Maxwellian velocity distribution with  $v_0=220$  km/s and  $v_{esc}=544$  km/s). The rates of WIMP-induced events due to spin-independent interaction cannot be larger than the residual spectrum. The quenching function in Ge is evaluated with the TRIM software which matches well with existing data[10]. As illustration,  $\chi$ N recoil spectrum due to an allowed (excluded)  $\sigma_{\chi N}^{SI}$  at  $m_\chi=7$  GeV is shown in the inset of Figure 3. Exclusion plot of  $\sigma_{\chi N}^{SI}$  versus  $m_\chi$  is displayed in Figure 4. Bounds from other benchmark experiments are superimposed[5, 7, 14]. An order of magnitude improvement is achieved compared to our previous results[4]. Part of the DAMA, CRESST-II and CoGeNT allowed regions are probed and excluded. We note that an excess remains in the sub-keV region not yet accounted for in this analysis, the understanding of which is the theme of our on-going investigations.

Studies continue on PPCGe and NPCGe at KSNL. Projects on improvement of electronics and sub-noise-edge analysis[12] are being pursued. Dedicated dark matter experiment CDEX with sub-keV germanium detectors are taking data at the new China Jinping Underground Laboratory (CJPL)[15]. This facility provides the attractive features such as a rock overburden exceeding 2400 m and horizontal drive-in access.

This work is supported by the Academia Sinica Investigator Award 2011-15, contracts 99-2112-M-001-017-MY3 from the National Science Council, Taiwan, and 108T502 from TÜBİTAK, Turkey.

\* Corresponding Author: htwong@phys.sinica.edu.tw

- [1] M. Drees and G. Gerbier, Review of Particle Physics Phys. Rev. **D 86**, 289 (2012), and references therein.
- [2] Q. Yue et al., High Energy Phys. and Nucl. Phys. **28**, 877 (2004); H.T. Wong et al., J. Phys. Conf. Ser. **39**, 266 (2006).
- [3] P.N. Luke et al., IEEE Trans. Nucl. Sci. **36**, 926 (1989); P.A. Barbeau, J.I. Collar and O. Tench, JCAP **09**, 009 (2007).
- [4] H.T. Wong, Mod. Phys. Lett. **A 23**, 1431 (2008); S.T. Lin et al., Phys. Rev. **D 79**, 061101(R) (2009).
- [5] C.E. Aalseth et al., Phys. Rev. Lett. **101**, 251301 (2008); C.E. Aalseth et al., Phys. Rev. Lett. **106**, 131301 (2011); C.E. Aalseth et al., Phys. Rev. Lett. **107**, 141301 (2011); C.E. Aalseth et al., arXiv:1208.5737 (2012).
- [6] For example, D. Hooper, Phys. Dark Univ. **1**, 1 (2012), and references therein; C. Kelso, D. Hooper and M.R. Buckley, Phys. Rev. **D 85**, 043515 (2012).
- [7] D.S. Akerib et al., Phys. Rev. **D 82**, 122004 (2010); Z. Ahmed et al., Phys. Rev. Lett. **106**, 131302 (2011); J. Angle et al., Phys. Rev. Lett. **107**, 051301 (2011); E. Aprile et al., Phys. Rev. Lett. **109**, 181301 (2012); Z. Ahmed et al., arXiv:1203.1309 (2012).
- [8] J.I. Collar, arXiv:1010.5187 (2010); arXiv:1103.3481 (2011); arXiv:1106.0653 (2011); J.I. Collar and N.E. Fields, arXiv:1204.3559 (2012).
- [9] H.B. Li et al., Phys. Rev. Lett. **90**, 131802 (2003); H.T. Wong et al., Phys. Rev. **D 75**, 012001 (2007); M. Deniz et al., Phys. Rev. **D 81**, 072001 (2010).
- [10] S.T. Lin et al., arXiv:0712.1645v4 (2007).
- [11] U. Tamm, W. Michaelis, and P. Coussieu, Nucl. Instrum. Meth. **48**, 301 (1967); M.G. Strauss and R.N. Larsen, Nucl. Instrum. Meth. **56**, 80 (1967); E. Sakai, IEEE Trans. Nucl. Sci. **18**, 208 (1971).
- [12] H.T. Wong, Int. J. Mod. Phys. **D 20**, 1463 (2011).
- [13] E. Aguayo et al., arXiv:1207.6716 (2012).
- [14] R. Bernabei et al., Eur. Phys. J. **C 67**, 39 (2010); M. Felizardo et al., Phys. Rev. Lett. **108**, 201302 (2012); G. Angloher et al., Eur. Phys. J. **C 72**, 1971 (2012); S. Archambault et al., Phys. Lett. **B 711**, 153 (2012).
- [15] K.J. Kang et al., J. Phys. Conf. Ser. **203**, 012028 (2010); Q. Yue and H.T. Wong, J. Phys. Conf. Ser. **375**, 042061 (2012).